electronics

MDPI

Article

Modeling and Investigation of Rear-Passivated Ultrathin CIGS Solar Cell

Nour El I. Boukortt [1,*], Salvatore Patanè [2] and Mabrouk Adouane [3]

[1] Electronics and Communication Engineering Department, Kuwait College of Science and Technology, Road N. 7, Doha 13113, Kuwait
[2] Department of Mathematics and Computer Science, Physics and Earth Science (MIFT), University of Messina, Viale F. Stagno d'Alcontres, 31, 98166 Messina, Italy
[3] Energy and Building Research Center, Kuwait Institute for Scientific Research (KISR), Safat 13109, Kuwait
* Correspondence: n.boukortt@kcst.edu.kw

Abstract: In this paper, we use numerical simulations to investigate ultrathin Cu $(In_{1-x}Ga_x)$ Se_2 solar cells. In the first part, we focus on the cell configuration in which the PV parameters fit and match the fabricated cell characteristics. Our goal is to investigate the impact of different loss mechanisms, such as interface trap density (D_{it}) and absorber trap density (N_t), in different cell pitch sizes on cell performances. D_{it} defines the number of carrier traps at CIGS/Al_2O_3 interfaces to recombine with photogenerated carriers. N_t defines the number of carrier traps in the absorber layer. Recombination through traps has been found to be the primary loss process in the investigated cell. Additional numerical simulations reveal appreciable gains in cell performance for various cell pitch sizes, absorber doping densities, Ga content, and graded bandgap under AM1.5 illumination. Research during the recent decade has clarified that the most promising strategy to achieve maximum efficiency consists of the so-called tandem configuration. Therefore, we here propose a u-CIGS/PERT silicon device employing, as a top cell, a u-CIGS cell optimized to take into account the above procedure. The results of these simulations provide insights into the optimization of ultrathin-film CIGS solar cells.

Keywords: thin film; traps; ultrathin CIGS; PERT silicon; device optimization

check for updates

Citation: Boukortt, N.E.I.; Patanè, S.; Adouane, M. Modeling and Investigation of Rear-Passivated Ultrathin CIGS Solar Cell. *Electronics* **2023**, *12*, 758. https://doi.org/10.3390/electronics12030758

Academic Editors: Kent Bertilsson and Emad Samadaei

Received: 13 January 2023
Revised: 29 January 2023
Accepted: 30 January 2023
Published: 2 February 2023

Copyright: © 2023 by the authors. Licensee MDPI, Basel, Switzerland. This article is an open access article distributed under the terms and conditions of the Creative Commons Attribution (CC BY) license (https://creativecommons.org/licenses/by/4.0/).

1. Introduction

The ultrathin-film Cu $(In_{1-x}Ga_x)$ Se_2 solar cell has significantly advanced, achieving high conversion efficiencies of over 12% [1–3]. In terms of production, the ultrathin CIGS PV manufacturing costs are expected to decrease as a result of high efficiency [4,5]. Recently, the CIGS devices have been improved by developing growth conditions and device engineering [6]. However, controlling the defect density of the absorbing layer is a crucial issue for the development of highly efficient and stable u-CIGS solar cells [6]. The u-CIGS solar cell performances are generally limited by several factors, including Grain Boundary (GB) defects, bulk traps, and interface traps [7]. The above factors lead to a higher recombination rate and lower charge carrier separation [7–10].

The ultrathin CIGS structures with Al_2O_3 rear surface passivation layer were investigated and optimized by Jackson, Bart, Joel, and our research group [1,8–10]. Kotipalli's group has reported that decreasing the deep-defect states can improve cell performance [11]. Several works reported different strategies to reduce the rear surface recombination which consist of implementing a very thin oxide layer and using different contact materials on the rear side of the cells [12–26]. Furthermore, ultrathin CIGS devices have drawn great attention because they could be most suitable for tandem cell applications as top and/or bottom cells with silicon (PERT, PERC, IBC, and a-Si:H) and perovskite solar cells [8,27]. Perovskite/CIGS tandem solar was investigated by Sining [24]. In addition, 2-Terminal

CIGS-perovskite cell devices have been successfully investigated by Jacobson and our research team [25,26].

In this work, we describe possible limitations and pathways to enhance cell performance. We evaluate scenarios in which u-CIGS could be optimized and used for high efficiencies. First, the proposed rear passivated ultrathin CIGS model was performed according to the fabricated cell [1]. Then, we studied the effect of the interface trap at the CIGS/Al_2O_3 interface, trap density in the absorber layer, and absorber doping density at different cell pitch sizes on cell performance. Further simulations quantify significant improvements in cell performance for absorber doping densities, Ga content, and graded bandgap at a fixed opening width in the Al_2O_3 layer. Finally, the optimized single u-CIGS cell has been used as a top cell for tandem configuration with the PERT silicon cell which arose recently as a very promising approach for achieving maximum efficiencies. The simulation results from these investigations are compared to the experimental results [1,26,27].

2. Device Structure

In this section, we describe a few features that are unique to our model. All our ultrathin CIGS models were performed using 2-D Silvaco tools. The simulated structure follows the design of the fabricated device [1]. The proposed model was inspired by Jackson's work [1]. In their study, Jackson et al. investigated the back-contact grid size in Al_2O_3 rear passivation ultrathin CIGS with an absorber layer of 500 nm-thick. Good agreement between simulated and reference quantities is observed [1]. Reducing the absorber thickness allows for minimizing the bulk defects, thereby improving overall recombination losses [1]. Figure 1 represents the studied model with the following configuration: ZnO:Al/ZnO/CdS/u-CIGS/Al_2O_3/Mo/glass-substrate (2 μm cell pitch). The thermionic emission and tunneling mechanisms are activated at the CdS/CIGS interface. Aluminum oxide (Al_2O_3) material of 25 nm-thick is used to reduce the recombination losses at the rear contact CIGS/Mo. A fixed negative charge density (Q_f, -1×10^{12} cm^{-2}) was implemented in the back passivation layer by introducing a single uniformly distributed acceptor into most of the Al_2O_3 layer. According to the literature, the front and rear contacts are assumed to be Schottky (4.7 eV) and ohmic, respectively [5,6]. The contact resistance for passivated cells has been approximated by Jackson to be 0.181 $\Omega \cdot$cm^2 for 0.1 ratio cell configuration [1]. The interface trap density (D_{it}) is inserted into the model by donor-type Gaussian defect distribution at CIGS/Al_2O_3 interface [1]. Figure 2 shows a band diagram of the calibrated model. Different band alignments can significantly contribute to carrier transport and recombination, as well as cell performance. Figure 3 shows energy band diagrams for the u-CIGS device simulated under illumination for different voltages. The forward applied voltage ranges between 0 V and 0.7 V. Furthermore, a 0.05 eV spike-like jump in the conduction band is generated at the CdS/CIGS heterojunction. The spike-like configuration occurs when the conduction band minimum of the absorber layer is smaller than the conduction band minimum of the buffer layer. This configuration is critical as, if the spike is sufficiently higher, it will prevent the flow of photogenerated carriers at the heterojunction interface, resulting in lower cell efficiency.

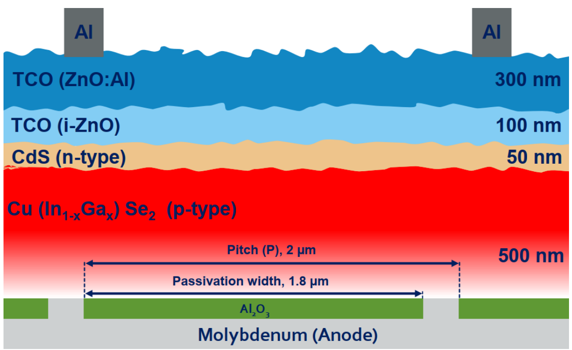

Figure 1. Structure of 2D passivated u-CIGS solar cell model.

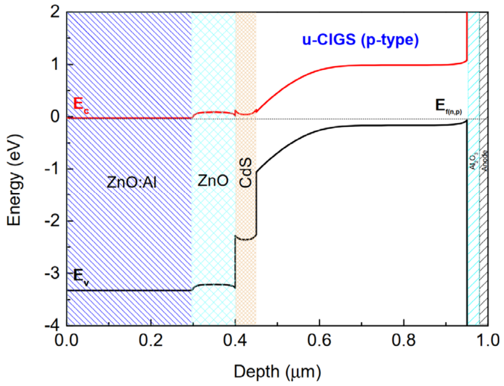

Figure 2. Schematic band diagram of ultrathin CIGS solar cell in dark conditions and equilibrium.

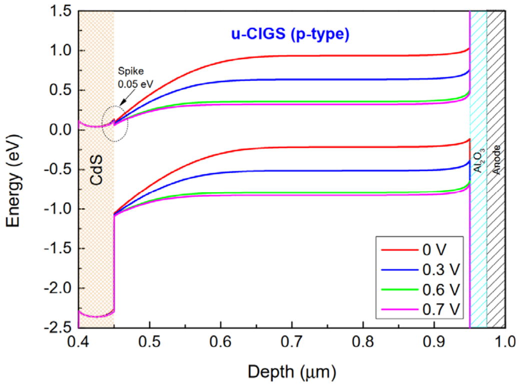

Figure 3. Band diagram of an ultrathin CIGS solar cell under different bias conditions (under illumination).

3. Results and Discussion

3.1. Model Validation

Figure 4 shows the simulated J–V characteristics and the external quantum efficiency (EQE) obtained at room temperature under the AM1.5G spectrum for the cell described in ref [1]. A rear contact resistance (R_c = 0.181 $\Omega\cdot cm^2$) is used to emulate the series resistance (R_s). The rear-passivated regions maintain a surface recombination velocity, S_{pass}, of 10^2 cm/s [1]. The cell characteristics of the investigated models J_{sc}, V_{oc}, FF, and η are compared to the experimental outputs [1] and presented in Table 1.

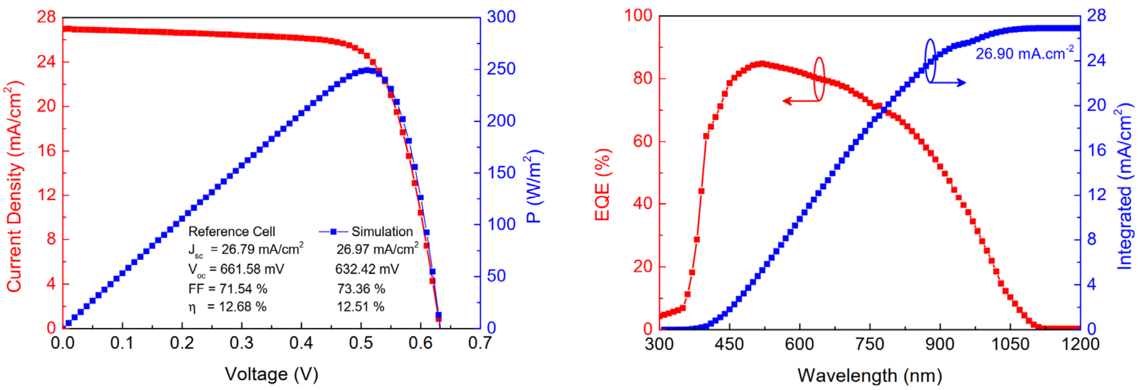

Figure 4. J–V curve, power, EQE spectrum, and integrated current density of the calibrated u-CIGS model, as Ref. [1].

Table 1. Investigated model characteristics.

PV Parameters	This Work Pass. $Q_f = -1 \times 10^{12}$ cm^{-2}	Ref. Cell [1] $Q_f = -1 \times 10^{12}$ cm^{-2}
J_0 (mA/cm^2)	3.85×10^{-6}	2.01×10^{-6}
J_{sc} (mA/cm^2)	26.97	26.79
V_{oc} (mV)	632.42	661.58
P_{max} (W/m^2)	250.32	-
FF (%)	73.36	71.54
η (%)	12.51	12.68

3.2. Influence of Interface Trap Density (D_{it})

As in our previous investigation, we demonstrated that the simulations fit well with the experimental results, and we have not changed the cell configuration. The rear passivation area is the parameter that expresses how much the ultrathin CIGS cell structure emphasizes the cell features. Cell pitch has been found to be important for the performance of the passivated cells. Here, we introduce the D_{it} in the CIGS/Al_2O_3 interface using the calibrated model configuration including a fixed charge $Q_f = -1 \times 10^{12}$ cm^{-2} [1] in the simulated models as a function of D_{it} and cell pitch that range from 0.5 µm to 4 µm, and from 1×10^{10} eV^{-1} cm^{-2} to 1×10^{13} eV^{-1}cm^{-2}, respectively, while Q_f and SRVs are kept constant. Figure 5 illustrates the influence of D_{it} on J_{sc}, V_{oc}, FF, and η when the cell pitch distance spans between 0.5 and 4 mm. The figure clearly highlights a strong dependence of J_{sc} on the cell pitch size. An increase in cell pitch contributes to an increase in the incoming photon absorption and current density, therefore current density increases, as well [9]. However, at a high cell pitch, a larger D_{it} dramatically degrades cell performance. The investigated ultrathin CIGS cell has two main recombination regions: CIGS bulk and rear passivation. This fact means the bulk doping density influences bulk resistivity (related to FF) and bulk lifetime (related to V_{oc}). Increasing cell pitch size leads to increased V_{oc}, indicating the recombination is reduced with a larger device pitch. At the highest D_{it} density (>1×10^{12} eV^{-1}cm^{-2}), the cell pitch variation has a very slight effect on V_{oc} due to less field-effect passivation strength compared to D_{it}, therefore high carrier recombination occurred in the rear side of the cell [10]. The FF decreases with cell pitch size due to an increase in R_s across the investigated cells [7,25]. Originally, the interface defect is assigned to the imperfect passivation; therefore, to maintain high performance, a suitable growth process should be able to ensure that the interface defect density is less than 10^{11} cm^{-2}. Moreover, it is worth noting that the efficiency has a maximum when the pitch is between one and two microns. Chemical passivation is improved by reducing D_{it} and/or SRV.

3.3. Influence of Trap Density (N_t)

Another key point to evaluate the cell performances consists of studying the effects of the absorber trap density with different energy levels for the donor trap. Following the previous results, we kept the interface defects density (D_{it}) constant at about 10^{11} eV^{-1}cm^{-2}. The thermionic and tunneling mechanisms are enabled at the absorber/buffer interface. In the absorber layer (CIGS, 1.15 eV), donor trapping centers are located at midgap (0.575 eV). They lie in a forbidden gap and exchange charge with the conduction and valence bands through the emission and capture of electrons. These trap levels will capture carriers, slowing the process of any solar cell. The trap centers influence the density of the space charge in CIGS bulk and the recombination statistics as illustrated in Figures 6 and 7. As shown in Figure 6, increasing N_t causes the offset of the valence and conduction bands to change. Additionally, the band-bending induced by the defect density influences the free carrier concentrations n and p, and, consequently, also the recombination current. In general, three recombination mechanisms often occur simultaneously in a semiconductor material: Shockley–Read–Hall (SRH), Auger, and radiative recombination. The total recombination rate is the sum of these three recombination rates [7,11].

$$\frac{1}{\tau_{total}} = \frac{1}{\tau_{SRH}} + \frac{1}{\tau_{Auger}} + \frac{1}{\tau_{rad}} \tag{1}$$

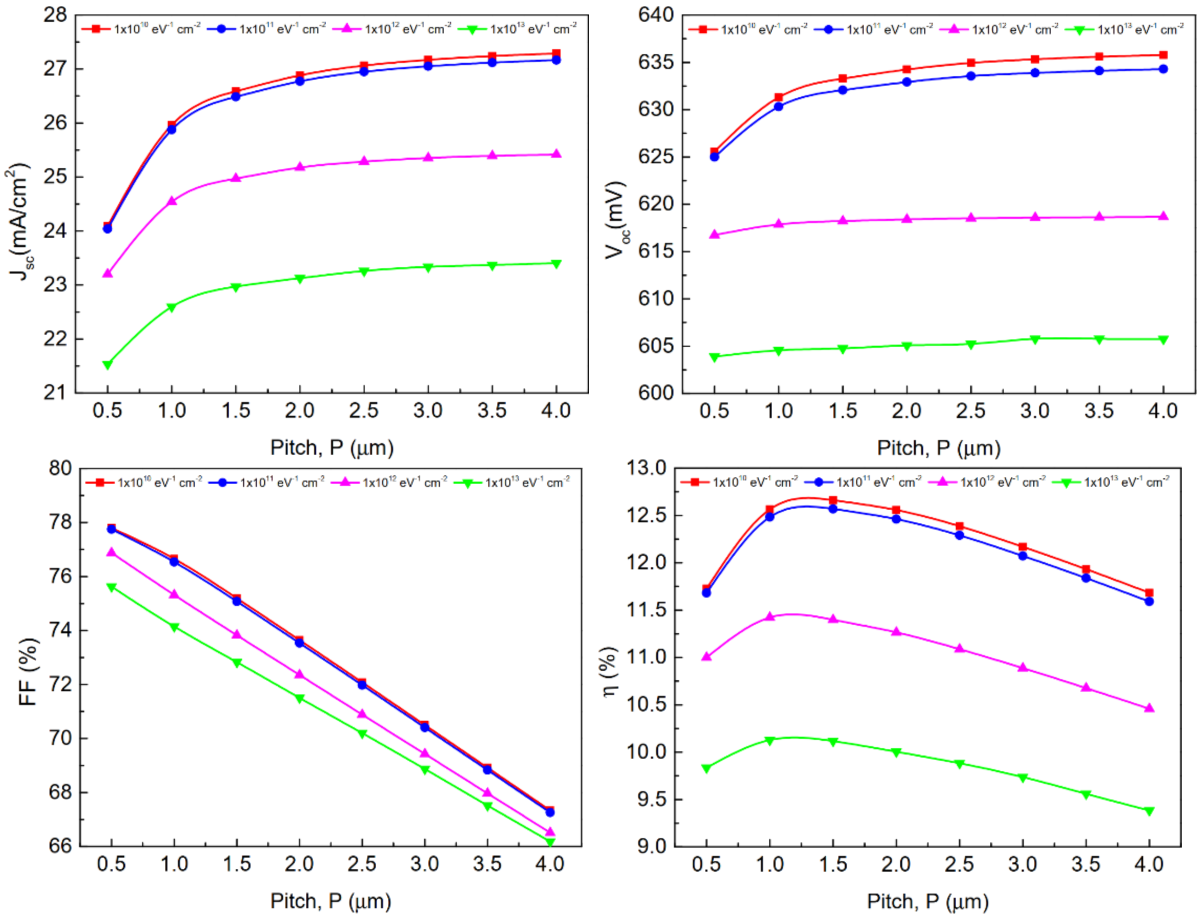

Figure 5. Cell parameters as a dependence of cell pitch extracted from 2D simulations for different chemical passivation D_{it}. The optimum pitch shifts from about 1 μm to 2 μm with a reduction in D_{it}. Lines are a visual guide.

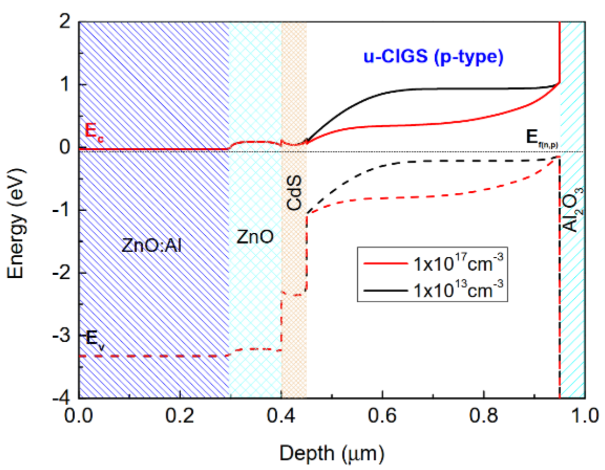

Figure 6. Schematic band diagram of ultrathin CIGS solar cell with two different absorber trap densities under illumination conditions—0 V Bias.

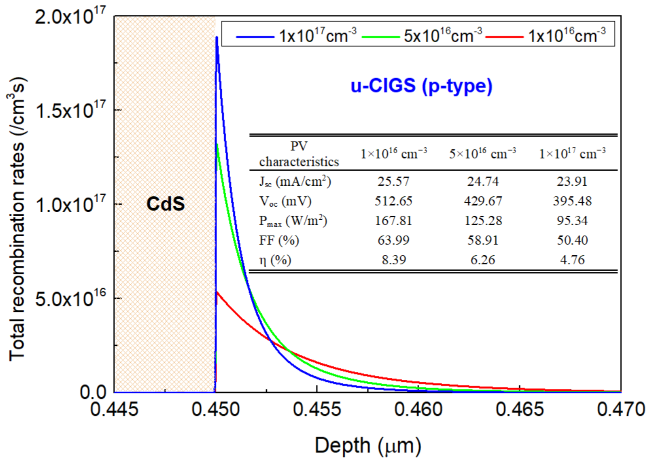

Figure 7. Recombination rates in ultrathin CIGS with different donor trap densities (N_t) at equilibrium—0 V Bias.

Auger electron and hole capture for the CIGS model is taken as 3.7×10^{-29} cm^6/s and 3.7×10^{-29} cm^6/s, respectively [7]. The radiative recombination coefficient for the CIGS material is taken as 1.5×10^{-10} cm^3/s [7].

The total recombination is proportional to the defect density near the CdS/CIGS interface as shown in Figure 7. When the cross-section area and trap density of electrons are increased, current density and cell efficiency decrease. Moreover, increasing the bulk defect density results in lower cell efficiencies that strongly depend on the capture cross sections and the trap energy levels. Figure 8 reports the effect on the cell performances of the absorber layer defects density (N_t) versus the defect's energy levels. Noticeably, shallow traps with energy below 0.3 eV have no significant effect on cell characteristics. Figure 9 shows the electric field distribution in ultrathin CIGS cells. Two spikes are observed at the heterojunctions: one at the CdS/CIGS junction and the other at the CIGS/Al_2O_3 interface. The presence of the spike at the CIGS/Al_2O_3 interface is due to the negative charges implemented in the rear-passivation layer preventing the minority carriers (electrons) to be recombined with the CIGS/Molybdenum interface traps. The maximum electric field observed is 0.118 MV/cm and 0.107 MV/cm for 10^{13} cm^{-3} and 10^{17} cm^{-3}, respectively. Table 2 illustrates the PV characteristics with different trap densities. We can conclude that inefficient charge transport and collection occurs at higher N_t, and with large energy levels of the trap, efficient transport is achieved if electrons are transported from CIGS to ZnO:Al without significant energy loss.

Table 2. PV characteristics with different absorber defect densities at a fixed energy level (0.4 eV).

PV Parameters	1×10^{13} cm^{-3}	1×10^{16} cm^{-3}	5×10^{16} cm^{-3}	1×10^{17} cm^{-3}
J_{sc} (mA/cm^2)	26.97	25.57	24.74	23.91
V_{oc} (mV)	632.40	512.65	429.67	395.48
P_{max} (W/m^2)	249.77	167.81	125.28	95.34
FF (%)	73.22	63.99	58.91	50.40
η (%)	12.48	8.39	6.26	4.76

3.4. Influence of Absorber Doping Density

It is well known that a thin absorber layer with a high doping concentration is not beneficial for a solar cell since poor light absorption entails lower η values. Similarly, a thicker absorber is also not suitable as it introduces a more significant route to transfer the photo-generated charge carriers that lead to high recombination. Therefore, an optimum u-CIGS absorber doping concentration selection is necessary for an efficient u-CIGS solar cell. The above states that the photovoltaic parameters (J_{sc}, V_{oc}, FF, and η) of a passivated u-CIGS solar cell are strongly influenced by the doping concentration of the absorber and cell pitch. We look for the optimum design varying, the doping concentration, and cell pitch size from 10^{14} to 10^{18} cm^{-3} and from 0.5 to 4 µm, respectively. Figure 10 shows obtained PV parameters for a passivated cell at fixed opening width (W = 200 nm) with contact resistance (R_c = 0.181 $\Omega \cdot cm^2$) at Mo/CIGS interface within the opening, as well as for the passivated layer with a specific Q_f value -1×10^{12} cm^{-2} and a fixed SRV value of 10^2 cm/s at CIGS/Al_2O_3 interface [1]. Figure 11 illustrates the effect of absorber layer doping density on the built-in electric field and total recombination rate using the 1×10^{14} cm^{-3}, 1×10^{16} cm^{-3}, and 1×10^{18} cm^{-3} u-CIGS absorber layer doping density. As compared to the 1×10^{16} cm^{-3}, the 1×10^{14} cm^{-3}, this doping density gives a weaker electric field which reduces the charge separation ability of the u-CIGS and, in turn, increases the charge recombination. When the doping density is lower and the cell pitch size is less than 2 µm, the J_{sc} of the passivated cells is improved. By increasing the cell area, a significant impact of the field-effect passivation compared to the bulk defect effect on cell performance is observed. However, we find that its value increases until it reaches a plateau after 2.5 µm. It is observed that the increase in J_{sc} is due to a decrease in the effective recombination with cell pitch. As the cell pitch increases for the low doping densities of the absorber, V_{oc} follows the same trend because of the improved charge separation. Increasing the doping density, the cell pitch effect starts reducing, and the V_{oc} value reaches 656 mV. Due to increasing in series resistance across the cell as the cell pitch size increases, FF follows the opposite trend of J_{sc} and V_{oc}. Increasing the absorber carrier concentration reduces the series resistance which increases the FF. The resulting cell conversion efficiency is a combination of J_{sc}, V_{oc}, and FF parameters; the first increases from small cell pitch, passes by an optimum value, and then decreases when the cell pitch size is further increased. These results are very important when designing an ultrathin solar cell to reduce production costs. Figure 12 shows the effect of the absorber doping density on cell efficiency at 1.5 µm cell pitch. The conversion efficiency reaches a maximum value of 13.07% at 1×10^{16} cm^{-3}, even though it starts decreasing afterward. A 120 nm thick MgF_2 layer has been used as an anti-reflective coating (ARC) to reduce the light reflection, thus enhancing efficiency [9]. Figure 13 illustrates a comparison of the J–V characteristics of the proposed u-CIGS models with and without ARC layers. Table 3 presents a comparison between simulated and fabricated model results at room temperature, AM1.5G spectrum [10,12].

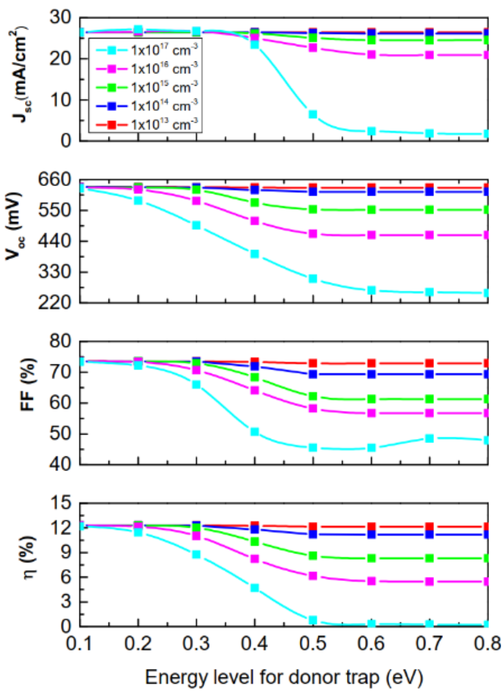

Figure 8. Cell parameters as a dependence of energy level for acceptor trap from 2D simulations for different defect densities.

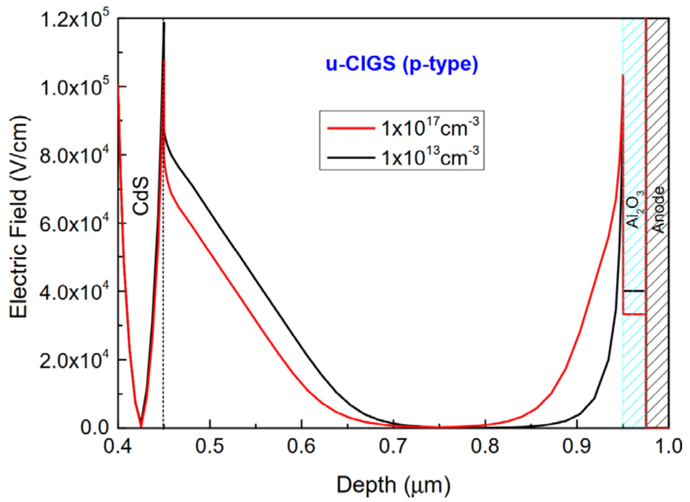

Figure 9. Electric Field comparison for two different donor trap densities (N_t) in ultrathin CIGS devices at equilibrium—0 V Bias.

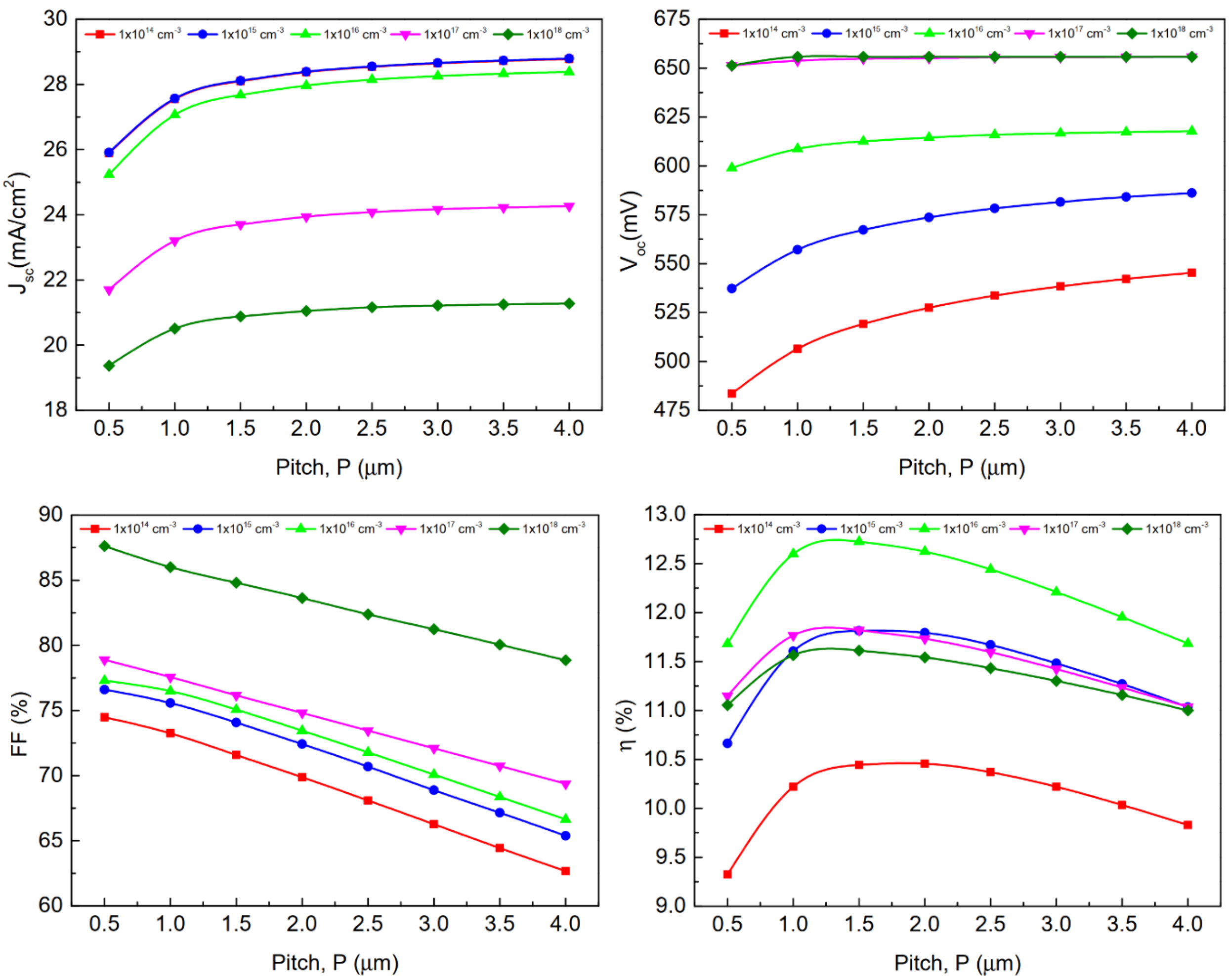

Figure 10. PV characteristics of u-CIGS cells for different cell pitches and different absorber doping densities.

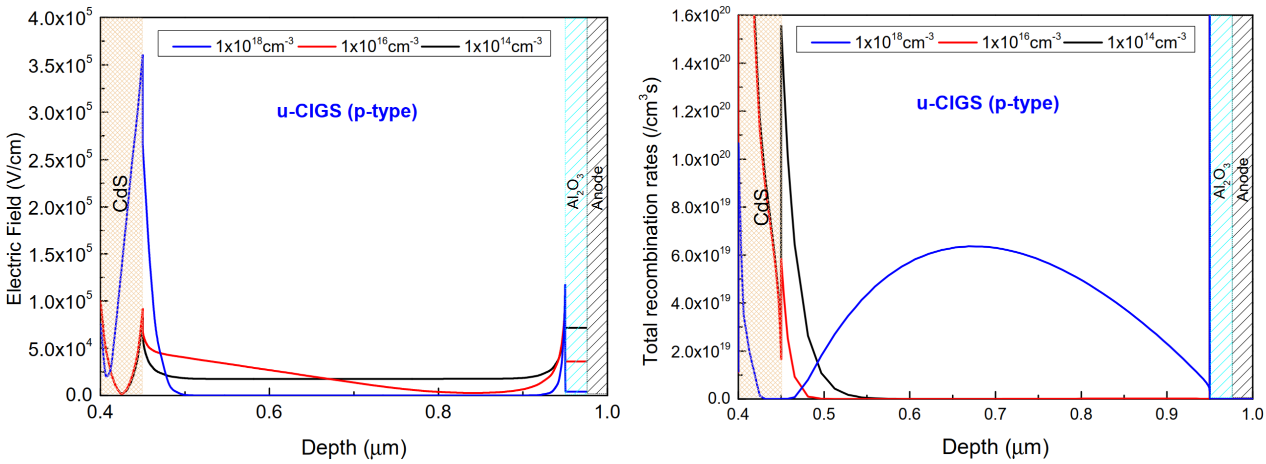

Figure 11. Effect of doping density in u-CIGS absorber on built-in electric field and total recombination rates at the CdS/u-CIGS and u-CIGS/Al_2O_3 interfaces under illumination—0 V Bias.

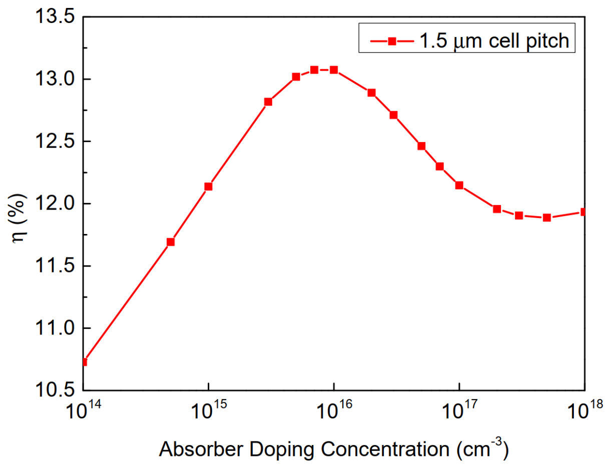

Figure 12. Conversion efficiency versus absorber doping concentration at cell pitch of 1.5 μm.

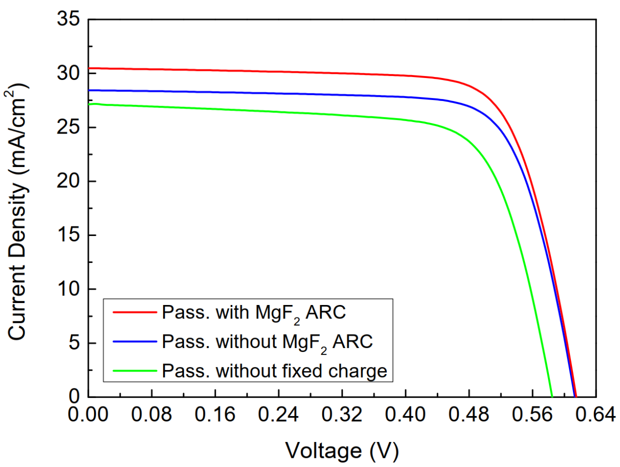

Figure 13. Simulated J–V curves of different u-CIGS solar cell models (d_{CIGS} = 500 nm, W = 200 nm, p = 1.5 μm, and D_{it} of 1×10^{10} $eV^{-1}cm^{-2}$).

Table 3. PV characteristics of different u-CIGS models.

PV Parameters	Opt. Cell with ARC	Opt. Cell w/o ARC	Opt. Pass. w/o Q_f	Ref. [1] Pass. with $-Q_f$	Ref. [10] Pass. with $-Q_f$
J_{sc} (mA/cm^2)	30.47	28.44	27.17	26.79	28.56
V_{oc} (mV)	615.04	613.22	584.63	661.58	625.5
P_{max} (W/m^2)	209.81	196.09	170.81	-	-
FF (%)	74.62	74.95	71.66	71.54	74.85
η (%)	14	13.07	11.38	12.68	13.37

3.5. Strategies to Improve the Efficiency of u-CIGS Solar Cells

In this section, we investigate different ways to improve cell performance by optimizing the spectral responses. Bandgap profile grading and tandem structure configuration are considered very promising approaches for achieving maximum efficiencies.

3.5.1. Impact of Ga-Concentration in u-CIGS Solar Cells

For the passivated u-CIGS solar cell, the photovoltaic parameters such as J_{sc}, V_{oc}, FF, and η are strongly influenced by the Ga/(In+Ga) ratio in $CuIn_{1-x}Ga_xS_2$ based solar cells as the CIGS alloy has both bandgap and electron affinity depending on the gallium content [9]. Previous modeling research has suggested that Ga composition grading is the most effective way to boost the efficiency of the next CIGS generation cells [3,27]. Following the above, we modulated the energy bandgap of the absorbing layer by changing the Ga/(In+Ga) ratios. The initial increase in efficiency is mainly due to an increase in the Ga content in the absorber layer, which also results in an increase in V_{oc} and a small increase in J_{sc}. The increase of J_{sc} is believed to be due to a reduction of the conduction band offset at the CdS/CIGS interface. In Figure 14, the characteristics of the cell when the Ga content spans between 12% and 77% are shown. It has been found that when the CIGS layer thickness is below 1 μm, an increase in Ga/(In+Ga) ratio towards the back contact improves the cell efficiency [6,9]. The efficiency reaches a maximum value when the Ga/(In+Ga) ratio at the junction reaches 77% (1.6 eV) [28]. The material properties are certainly very significant for future tandem structures where bandgap matching with the optical spectrum can be further exploited to increase efficiency [2].

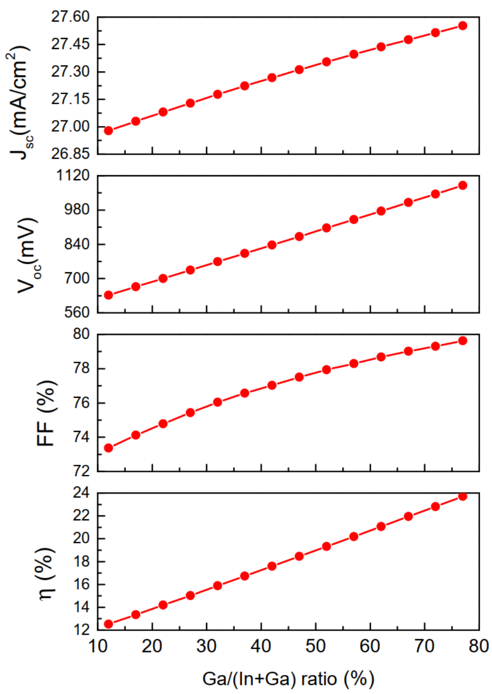

Figure 14. Cell parameters for different Ga/(In+Ga) ratios.

3.5.2. Impact of Stepped Bandgap Profile and Ga-Concentration in u-CIGS Solar Cells

We investigated the effect of the thickness of the sub-layers on cell performance. The proposed device consists of three layers with thicknesses of 50, 150, and 300 nm, and with a bandgap of 1.6 eV, 1.15 eV, and 1.32 eV, respectively, as illustrated in Figure 15. Many research works clarified that reduced absorber thickness leads to a decrease in the photon absorption rate and consequently less amount of the generated carriers [3–7]. A decrease in the photocurrent density results inevitably in a drop in the yields of solar cell devices. In this frame, we assumed that an optimal thickness exists and simulated the effect of the sub-absorber thickness on the cell characteristics by varying the thickness of layer one and layer three one at a time by keeping the total thickness of the absorber at 500 nm (See Figure 16). A strong impact on the cell parameters appears with a thickness greater than 200 nm in both cases. The optimal sub-layer thicknesses were found to increase the conversion efficiency from 13.07% to 15.82%. These consist of the following configuration: CIGS 1 (300 nm)/CIGS 2 (150 nm)/CIGS 3 (50 nm). After optimizing the thickness of the sub-layers, it is very important to optimize the bandgap of the second sublayer (CIGS 2). Figure 17 presents the cell characteristics' dependence on Ga content in CIGS 2 from 12% to 77%. Improvements in J_{sc} and FF were clearly visible while increasing the Ga content due to conduction band offset reduction at CIGS 1/CIGS 2 interface. After following the same trend until a certain concentration level, η then becomes approximately constant from 60% of the Ga/(In+Ga) ratio. An improvement in V_{oc} has been found when the Ga content ratio ranges between 30% and 60%. In conclusion, we chose as the optimum value the Ga content ratio of 57% corresponding to an energy gap of 1.46 eV. Figure 18 illustrates the electric field distribution, electron velocity, electron concentration inside the investigated structure, and J-V characteristics with two different absorber configurations. For the $E_{g1} < E_{g2} < E_{g3}$ absorber configuration, an increase in the current density is observed due to high electric field distribution across the junction. On the other hand, the configuration $E_{g1} > E_{g2} > E_{g3}$ shows high electron velocity and concentration that cause a loss in short circuit current due to lower electric field strength at higher E_g that, in turn, causes higher carriers' recombination within the absorber layer.

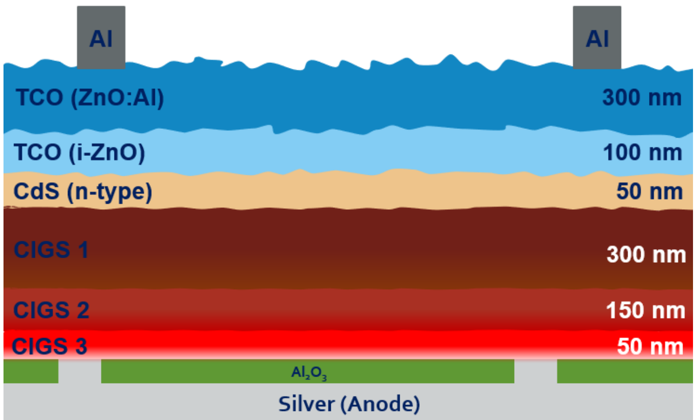

Figure 15. Schematic structure of ultrathin CIGS solar cell with three sub-layers.

3.5.3. Optimization of u-CIGS/C-Si PERT Tandem Solar Cell

The numerical simulations were performed to design a two-terminal u-CIGS/silicon tandem cell targeting the best efficiency and stability [8,26]. The proposed C-Si PERT model was inspired by Benick's works [27]. The PERT cell model was calibrated with the reported experimental data [27]. In their study, Benick et. al. applied ion implantation for the realization of both the emitter and the back surface field (BSF) of high-efficiency PERT and PERL structures [27]. For the C-Si model, good agreement between simulated and reference quantities has been obtained in previous work [26]. Figure 19 represents the investigated u-CIGS/C-Si PERT tandem cell with the following configuration: MgF_2/ZnO:Al/ZnO/CdS/u-CIGS/ITO/FSF/Bulk/BSF/Al_2O_3/Silver/glass-substrate.

The thermionic emission and tunneling mechanisms at the CdS/CIGS interface are activated in the simulation. An aluminum oxide (Al_2O_3) material of 10 nm-thick has been used for the rear passivation and reduces the recombination losses at the rear Silicon/Silver contact. According to the literature, the front and rear contacts are assumed to be Schottky (4.7 eV) and ohmic contact, respectively. The interface trap density (D_{it}) is inserted into the model by donor-type Gaussian defect distribution at Silicon/Al_2O_3 interface [1]. The J–V curves of the studied cell models are shown in Figure 20. An efficiency of 29.93% can be obtained with the optimized 2T u-CIGS/Silicon tandem cell [29]. Table 4 summarizes the PV cell performance of the studied cells in comparison to recently published work [8,26,28].

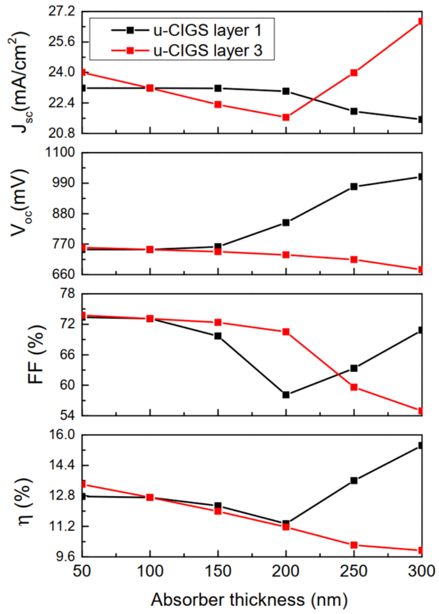

Figure 16. PV characteristics of u-CIGS cells for different sub-layer thicknesses.

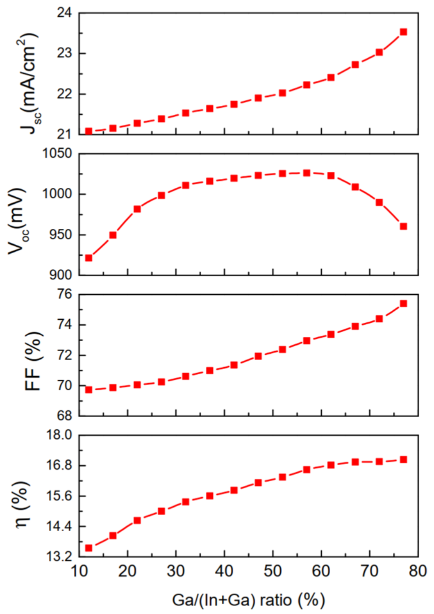

Figure 17. PV characteristics of u-CIGS cells for different Ga/(In+Ga) ratios for sub-layer (CIGS 2).

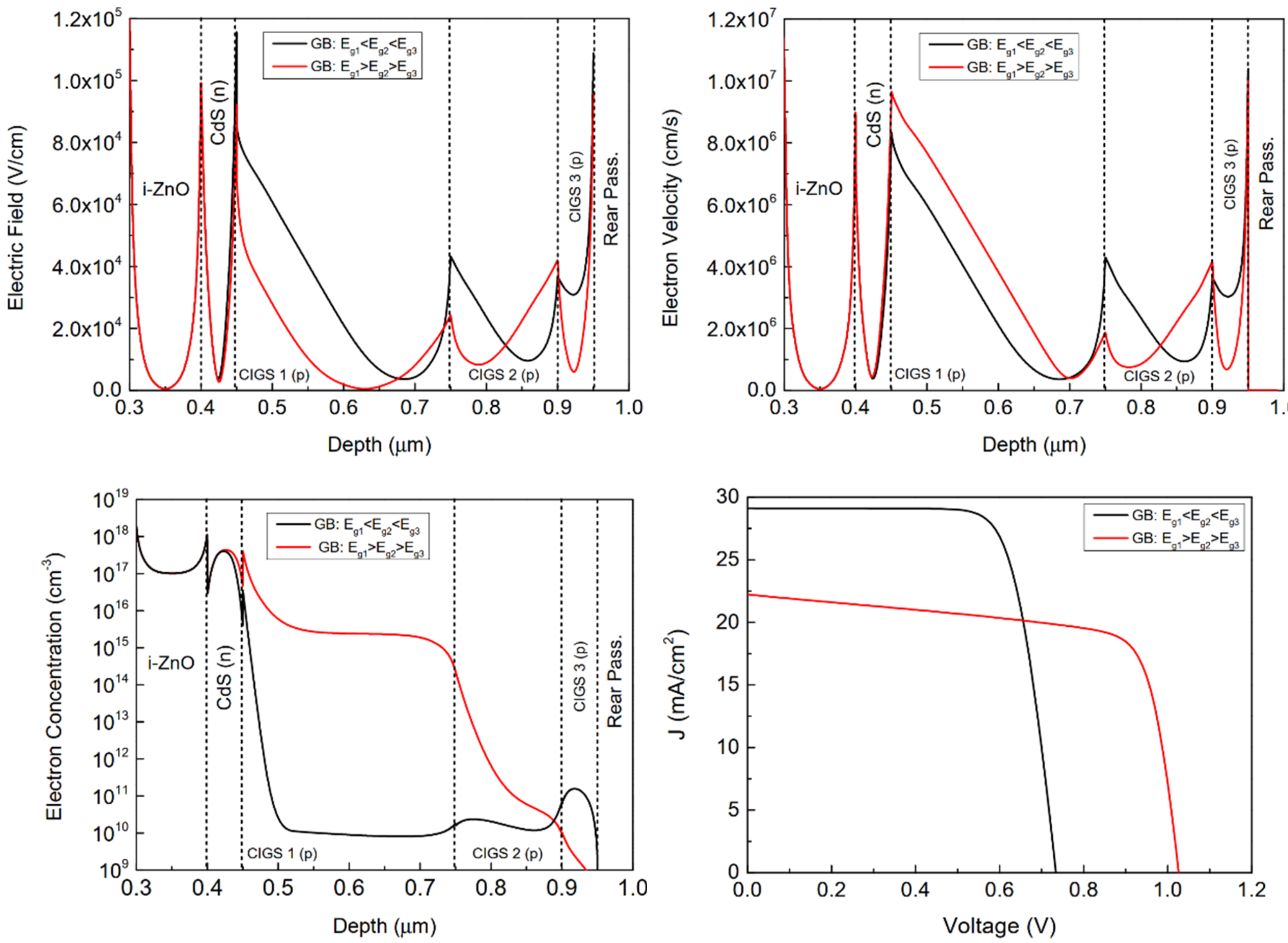

Figure 18. Electric field distribution, electron velocity, and electron concentration inside the u-CIGS structure. J–V characteristics with two different absorber configurations.

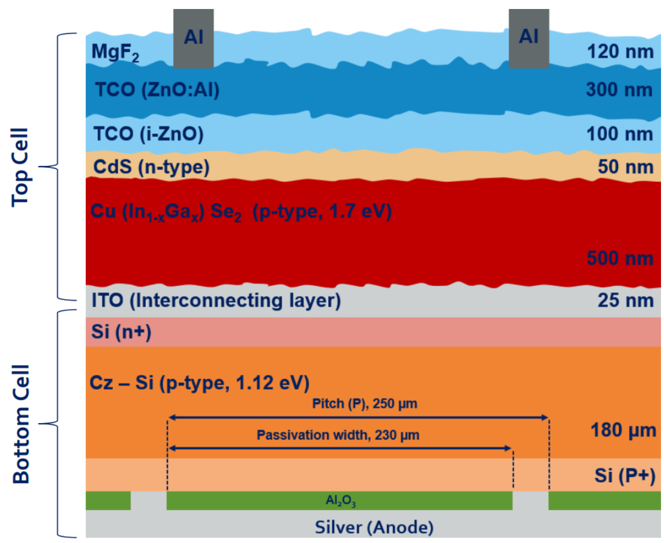

Figure 19. Schematic of optimized u-CIGS/C-Si PERT tandem solar cell.

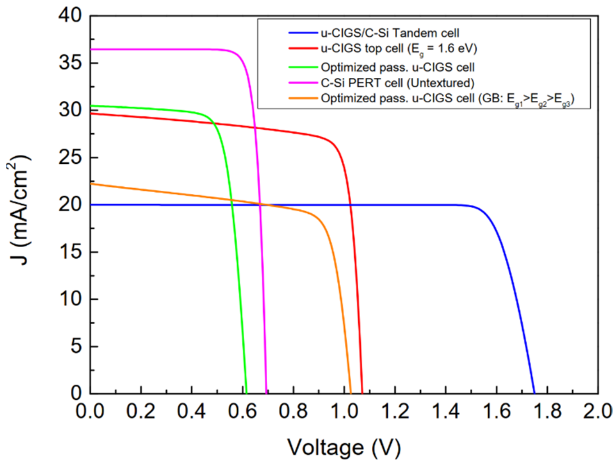

Figure 20. J–V curves of the optimized u-CIGS cells, C-Si PERT cell, and u-CIGS/C-Si PERT tandem solar cells at a fixed width grid of 25 μm.

Table 4. PV characteristics of different ultrathin CIGS cells.

Cell	Absorber Thickness	E_g (eV)	J_{sc} (mA/cm^2)	V_{oc} (V)	FF (%)	η (%)
Optimized pass. u-CIGS cell	500 nm	1.15	30.47	0.615	74.62	14
Optimized pass. u-CIGS cell (Thickness for graded Bandgap)	500 nm	1.6 eV/1.3 eV/1.15 eV	21.56	1.012	70.74	15.45
Optimized pass. u-CIGS cell (Graded Bandgap $E_{g1} > E_{g2} > E_{g3}$)	500 nm	1.6 eV/1.46 eV/1.15 eV	22.22	1.026	72.95	16.63
Optimized pass. u-CIGS cell (Graded Bandgap $E_{g1} < E_{g2} < E_{g3}$)	500 nm	1.15 eV/1.46 eV/1.6 eV	29.11	0.733	75.74	16.18
C-Si PERT cell untextured	180 μm	1.124	36.45	0.693	83.36	21.07
C-Si PERT cell textured [28]	~180 μm	-	40.9	0.691	83.8	22.7
u-CIGS top cell	500 nm	1.6	29.65	1.070	79.58	25.27
C-Si PERT filtered by top cell	100 μm	1.124	9.05	0.633	25.04	1.43
Our previous work [26] Perovskite/u-CIGS Tandem cell	500 nm/600 nm	1.6/1.15	20.89	1.708	85.05	30.36
u-CIGS/C-Si Tandem cell	500 nm/180 μm	1.6/1.124	19.98	1.749	85.57	29.93

4. Conclusions

In this paper, passivated u-CIGS solar cells were successfully simulated using TCAD tools. The investigation takes into account the effect of recombination loss mechanisms, such as interface trap density and absorber trap density, on the performance of u-CIGS solar cells. The influence of the cell pitch size and absorber doping density on cell performance has been investigated and analyzed under room temperature, AM1.5G spectrum. The results indicate that a correct optimization of the construction parameters improves the performance of the cell. In particular, we observed that excessive dimensions of the cell step, doping density, and trap density give rise to a higher total recombination rate of the carriers and, therefore, to reduced efficiency. Using the optimal values for these parameters and an MgF_2 layer as ARC, it was possible to simulate a device capable of exhibiting an efficiency of 14%. Attention was paid to the doping density of the absorber, the Gallium content, and the consequent bandgap variation. Furthermore, a cell consisting of an absorber with variable Ga content was simulated, assuming that the absorber consists of three layers with different thicknesses and bandgap values. The optimized cell was then used in the model of a tandem structure which employs a PERT-type silicon cell as the bottom cell. The approach used to optimize the overall efficiency paves the way for the design of highly efficient photovoltaic devices in tandem configuration with ultrathin film technology.

Author Contributions: Conceptualization, N.E.I.B.; methodology, N.E.I.B.; software, N.E.I.B.; validation, N.E.I.B., M.A. and S.P.; investigation, N.E.I.B.; writing—original draft preparation, N.E.I.B.; writing—review and editing, S.P. and M.A.; supervision, S.P. and M.A. All authors have read and agreed to the published version of the manuscript.

Funding: This project was supported by the Kuwait Foundation for the Advancement of Sciences (KFAS) under project codes: PN20-35EE-03.

Data Availability Statement: Not applicable.

Acknowledgments: This research work was also partially supported by the Semiconductor Laboratory (GE01/08), Kuwait University.

Conflicts of Interest: The authors declare no conflict of interest. The funders had no role in the design of the study; in the collection, analyses, or interpretation of data; in the writing of the manuscript, or in the decision to publish the results.

References

1. Lontchi, J.; Zhukova, M.; Kovacic, M.; Krc, J.; Chen, W.C.; Edoff, M.; Bose, S.; Salomé, P.M.; Goffard, J.; Cattoni, A.; et al. Optimization of Back Contact Grid Size in Al_2O_3-Rear-Passivated Ultrathin CIGS PV Cells by 2-D Simulations. *IEEE J. Photovolt.* **2020**, *10*, 1908–1917. [CrossRef]
2. Boukortt, N.E.I.; Patanè, S.; Hadri, B.; Crupi, G. Graded Bandgap Ultrathin CIGS Solar Cells (Invited Paper). *Electronics* **2023**, *12*, 393. [CrossRef]
3. Boukortt, N.E.I.; Adouane, M.; AlHammadi, R. High-performance ultrathin Cu(In,Ga)Se_2 solar cell optimized by silvaco tools. *Sol. Energy* **2021**, *228*, 282–289. [CrossRef]
4. Dhere, N.G. Toward GW/year of CIGS production within the next decade. *Sol. Energy Mater. Sol. Cells* **2007**, *91*, 1376–1382. [CrossRef]
5. Edoff, M.; Schleussner, S.; Wallin, E.; Lundberg, O. Technological and economical aspects on the influence of reduced Cu(In,Ga)Se_2 thickness and Ga grading for co-evaporated Cu(In,Ga)Se_2 modules. *Thin Solid Film.* **2011**, *519*, 7530–7533. [CrossRef]
6. Ochoa, M.; Buecheler, S.; Tiwari, A.N.; Carron, R. Challenges and opportunities for an efficiency boost of next generation Cu(In,Ga)Se_2 solar cells: Prospects for a paradigm shift. *Energy Environ. Sci.* **2020**, *13*, 2047–2055. [CrossRef]
7. Sravani, L.; Routray, S.; Courel, M.; Pradhan, K.P. Loss mechanisms in CZTS and CZTSe Kesterite thin-film solar cells: Understanding the complexity of defect density. *Sol. Energy* **2021**, *227*, 56–66. [CrossRef]
8. Boukortt, N.E.I.; Hadri, B. Simulation of electrical characteristics of PERC solar cells. *J. Electron. Mater.* **2018**, *47*, 5825–5832. [CrossRef]
9. Joel, J. Characterization of Al_2O_3 as CIGS Surface Passivation Layer in High-Efficiency CIGS Solar Cells. Master's Thesis, Uppsala University, Uppsala, Sweden, 2014.
10. Boukortt, N.E.I.; Patanè, S.; Adouane, M.; AlHammadi, R. Numerical optimization of ultrathin CIGS solar cells with rear surface passivation. *Sol. Energy* **2021**, *220*, 590–597. [CrossRef]
11. Kotipalli, R.; Vermang, B.; Fjällström, V.; Edoff, M.; Delamare, R.; Flandre, D. Influence of Ga/(Ga+ In) grading on deep-defect states of Cu(In,Ga)Se_2 solar cells. *Phys. Status Solidi (RRL)—Rapid Res. Lett.* **2015**, *9*, 157–160. [CrossRef]
12. Kotipalli, R.; Vermang, B.; Joel, J.; Rajkumar, R.; Edoff, M.; Flandre, D. Investigating the electronic properties of Al_2O_3/Cu (In Ga)Se_2 interface. *AIP Adv.* **2015**, *5*, 107101. [CrossRef]
13. Birant, G.; Mafalda, J.; Scaffidi, R.; De Wild, J.; Buldu, D.; Kohl, T.; Brammertz, G.; Meuris, M.; Poortmans, J.; Vermang, B. Rear surface passivation of ultra-thin CIGS solar cells using atomic layer deposited HfOx. *EPJ Photovolt.* **2020**, *11*, 10. [CrossRef]
14. Vermang, B.; Wätjen, J.T.; Frisk, C.; Fjällström, V.; Rostvall, F.; Edoff, M.; Salomé, P.; Borme, J.; Nicoara, N.; Sadewasser, S. Introduction of Si PERC Rear Contacting Design to Boost Efficiency of Cu(In,Ga)Se_2 Solar Cells. *IEEE J. Photovolt.* **2014**, *4*, 1644–1649. [CrossRef]
15. Vermang, B.; Rostvall, F.; Fjällström, V.; Edoff, M. Potential-induced optimization of ultra-thin rear surface passivated CIGS solar cells. *Phys. Status Solidi (RRL)—Rapid Res. Lett.* **2014**, *8*, 908–911. [CrossRef]
16. Boukortt, N.E.I.; Patanè, S. Single junction-based thin-film CIGS solar cells optimization with efficiencies approaching 24.5%. *Optik* **2020**, *218*, 165240. [CrossRef]
17. Cunha, J.M.; Rocha, C.; Vinhais, C.; Fernandes, P.A.; Salomé, P.M. Understanding the AC Equivalent Circuit Response of Ultrathin Cu(In,Ga)Se_2 Solar Cells. *IEEE J. Photovolt.* **2019**, *9*, 1442–1448. [CrossRef]
18. Bose, S.; Cunha, J.M.; Suresh, S.; De Wild, J.; Lopes, T.S.; Barbosa, J.R.; Silva, R.; Borme, J.; Fernandes, P.A.; Vermang, B.; et al. Optical lithography patterning of SiO_2 layers for interface passivation of thin film solar cells. *Sol. RRL* **2018**, *2*, 1800212. [CrossRef]
19. Cunha, J.M.V.; Fernandes, P.A.; Hultqvist, A.; Teixeira, J.P.; Bose, S.; Vermang, B.; Garud, S.; Buldu, D.; Gaspar, J.; Edoff, M.; et al. Insulator Materials for Interface Passivation of Cu(In,Ga)Se_2 Thin Films. *IEEE J. Photovolt.* **2018**, *8*, 1313–1319. [CrossRef]
20. Ledinek, D.; Salome, P.; Hägglund, C.; Zimmermann, U.; Edoff, M. Rear Contact Passivation for High Bandgap Cu(In,Ga)Se_2 Solar Cells With a Flat Ga profile. *IEEE J. Photovolt.* **2018**, *8*, 864–870.

21. Salome, P.M.; Vermang, B.; Ribeiro-Andrade, R.; Teixeira, J.P.; Cunha, J.M.; Mendes, M.J.; Haque, S.; Borme, J.; Aguas, H.; Fortunato, E.; et al. Passivation of interfaces in thin film solar cells: Understanding the effects of a nanostructured rear point contact layer. *Adv. Mater. Interfaces* **2018**, *5*, 1701101. [CrossRef]
22. Goffard, J.; Colin, C.; Mollica, F.; Cattoni, A.; Sauvan, C.; Lalanne, P.; Guillemoles, J.F.; Naghavi, N.; Collin, S. Light trapping in ultrathin CIGS solar cells with nanostructured back mirrors. *IEEE J. Photovolt.* **2017**, *7*, 1433–1441. [CrossRef]
23. Boukortt, N.E.I.; AlAmri, A.M.; Bouhjar, F.; Bouhadiba, K. Investigation and optimization of ultrathin Cu(In,Ga)Se_2 solar cells by using silvaco-TCAD tools. *J. Mater. Sci. Mater. Electron.* **2021**, *32*, 21525–21538. [CrossRef]
24. Yun, S.; Qin, Y.; Uhl, A.R.; Vlachopoulos, N.; Yin, M.; Li, D.; Han, X.; Hagfeldt, A. New-generation integrated devices based on dye-sensitized and perovskite solar cells. *Energy Environ. Sci.* **2018**, *11*, 476–526.
25. Jacobsson, T.J.; Hultqvist, A.; Svanström, S.; Riekehr, L.; Cappel, U.B.; Unger, E.; Rensmo, H.; Johansson, E.M.; Edoff, M.; Boschloo, G. 2-Terminal CIGS-perovskite tandem cells: A layer by layer exploration. *Sol. Energy* **2020**, *207*, 270–288. [CrossRef]
26. Boukortt, N.E.I.; Patanè, S.; Loureiro, A.G.; AlAmri, A.M.; Abdulraheem, Y.M.; Lenka, T.R.; Paul, R.; Abushattal, A. Electrical and Optical Investigation of 2T-Perovskite/u-CIGS Tandem Solar Cells with ~30% Efficiency. *IEEE Trans. Electron Devices* **2022**, *69*, 3798–3806. [CrossRef]
27. Benick, J.; Steinhauser, B.; Müller, R.; Bartsch, J.; Kamp, M.; Mondon, A.; Richter, A.; Hermle, M.; Glunz, S. High efficiency n-type PERT and PERL solar cells. In Proceedings of the 2014 IEEE 40th Photovoltaic Specialist Conference (PVSC), Denver, CO, USA, 8–13 June 2014; pp. 3637–3640.
28. de Wild, J.; Scaffidi, R.; Brammertz, G.; Birant, G.; Vermang, B. Dielectric Front Passivation for Cu(In,Ga)Se_2 Solar Cells: Status and Prospect. *Adv. Energy Sustain. Res.* **2022**, 2200132. [CrossRef]
29. Li, P.; Xiong, H.; Lin, L.; Jiang, L.; Kang, Z.; Yan, Q.; Lien, S.Y.; Chen, H.; Qiu, Y. Modeling and simulation of bifacial perovskite/PERT-silicon tandem solar cells. *Sol. Energy* **2021**, *227*, 292–302. [CrossRef]

Disclaimer/Publisher's Note: The statements, opinions and data contained in all publications are solely those of the individual author(s) and contributor(s) and not of MDPI and/or the editor(s). MDPI and/or the editor(s) disclaim responsibility for any injury to people or property resulting from any ideas, methods, instructions or products referred to in the content.